Title

Intravoxel incoherent motion diffusion-weighted MRI at 3.0 T differentiates malignant breast lesions from benign lesions and breast parenchyma.

Journal

Journal of Magnetic Resonance Imaging, 40(4)

Authors

Bokacheva, Louisa

Kaplan, Jennifer

Giri, Dilip

et al.

Publication Date

2014-10-01

DOI

10.1002/jmri.24462

Peer reviewed

HHS Public Access

Author manuscript

J Magn Reson Imaging. Author manuscript; available in PMC 2016 March 10.

Published in final edited form as:

J Magn Reson Imaging. 2014 October ; 40(4): 813–823. doi:10.1002/jmri.24462.

Intravoxel Incoherent Motion Diffusion-Weighted MRI at 3.0 T Differentiates Malignant Breast Lesions From Benign Lesions and Breast Parenchyma

Louisa Bokacheva, PhD[1], **Jennifer B. Kaplan, MD**[2], **Dilip D. Giri, MD**[3], **Sujata Patil, PhD**[4], **Merlin Gnanasigamani, MD**[2], **C. Gregory Nyman, RT**[2], **Joseph O. Deasy, PhD**[1], **Elizabeth A. Morris, MD**[2], and **Sunitha B. Thakur, PhD**[1,2,*]

[1]Department of Medical Physics, Memorial Sloan-Kettering Cancer Center, New York, NY, USA

[2]Department of Radiology, Memorial Sloan-Kettering Cancer Center, New York, NY, USA

[3]Department of Pathology, Memorial Sloan-Kettering Cancer Center, New York, NY, USA

[4]Department of Biostatistics, Memorial Sloan-Kettering Cancer Center, New York, NY, USA

Abstract

Purpose—To study the differentiation of malignant breast lesions from benign lesions and fibroglandular tissue (FGT) using apparent diffusion coefficient (ADC) and intravoxel incoherent motion (IVIM) parameters.

Materials and Methods—This retrospective study included 26 malignant and 14 benign breast lesions in 35 patients who underwent diffusion-weighted MRI at 3.0T and nine b-values (0–1000 s/mm^2). ADC and IVIM parameters (perfusion fraction f_p, pseudodiffusion coefficient D_p, and true diffusion coefficient D_d) were determined in lesions and FGT. For comparison, IVIM was also measured in 16 high-risk normal patients. A predictive model was constructed using linear discriminant analysis. Lesion discrimination based on ADC and IVIM parameters was assessed using receiver operating characteristic (ROC) and area under the ROC curve (AUC).

Results—In FGT of normal subjects, f_p was 1.1 ± 1.1%. In malignant lesions, f_p (6.4 ± 3.1%) was significantly higher than in benign lesions (3.1 ± 3.3%, $P = 0.0025$) or FGT (1.5 ± 1.2%, $P < 0.001$), and D_d ((1.29 ± 0.28) × 10^{-3} mm^2/s) was lower than in benign lesions ((1.56 ± 0.28) × 10^{-3} mm^2/s, $P = 0.011$) or FGT ((1.86 ± 0.34) × 10^{-3} mm^2/s, $P < 0.001$). A combination of D_d and f_p provided higher AUC for discrimination between malignant and benign lesions (0.84) or FGT (0.97) than ADC (0.72 and 0.86, respectively).

Conclusion—The IVIM parameters provide accurate identification of malignant lesions.

Keywords

diffusion-weighted imaging; intravoxel incoherent motion; breast cancer; benign breast lesions

*Address reprint requests to: S.B.T., Department of Medical Physics, Memorial Sloan-Kettering Cancer Center, 1275 York Ave., New York, NY 10065. thakurs@mskcc.org.

A subset of data used in this article was presented at the Annual Meeting of ISMRM 2012 in Melbourne, Australia.

DIFFUSION-WEIGHTED (DW) magnetic resonance imaging (MRI) and measurements of the apparent diffusion coefficient (ADC) have proven useful in the detection and characterization of cancer (1). The ADC is sensitive to tissue cellularity and is usually lower in malignant tumors, in which water diffusion is more restricted because of the increased cell density and reduced extracellular space compared to the normal tissue. DW images may also reflect perfusion effects, as the microscopic blood flow in a randomly oriented capillary network creates a pseudodiffusion contribution to the DW signal. This effect, known as the intravoxel incoherent motion (IVIM) (2), has been observed in a variety of well-vascularized tissues, including brain, liver, pancreas, kidney, muscle, and placenta (3–8). The IVIM measurements have been reported in liver lesions (9), prostate cancer (10), and head and neck cancer (11,12) and used to differentiate pancreatic tumors (5) and salivary gland tumors (12). The IVIM component may reduce the accuracy of cancer differentiation using ADC by introducing a positive bias proportional to the perfusion fraction (13) into the ADC values and increasing their variability and dependence on the choice of the diffusion-weighting factors, or b-values (14,15). The b-value scheme also strongly affects the IVIM parameters and the separation between their values in cancer and normal tissue when the number of b-values is small (10). Therefore, the reliability of the IVIM measurements achievable in clinical practice and their usefulness in cancer diagnosis need to be further evaluated.

In the diagnosis of breast lesions, DW imaging may be used as an adjunct technique to the contrast-enhanced MRI, which provides high sensitivity, but limited specificity (16). Differentiation between malignant and benign breast lesions based on ADC has been shown to achieve a sensitivity of 85–95% and a specificity of 50–90% (15,17–21). Perfusion effects are negligible in the DW signal of normal breast parenchyma, as shown by Baron et al (22) in healthy volunteers, but can be appreciable in breast cancer (15,23). In patients with locally advanced breast cancer, Sigmund et al (24) found the average perfusion fraction in tumors to be about 10% (range, 3–22%) and demonstrated that the true diffusion coefficient provided a better separation between cancer and fibroglandular tissue (FGT) than the ADC. In agreement with Baron et al (22), Sigmund et al (24) found that the IVIM contribution in normal parenchyma was small; however, neither study reported the perfusion fraction values in FGT. Such estimates may be useful as a measure of robustness of the IVIM measurements.

The purpose of this study was to use DW MRI at 3.0 T and 1) measure the IVIM parameters in breast parenchyma in high-risk normal subjects and determine a range of b-values that provide reliable IVIM parameter estimates; 2) determine the IVIM parameters in malignant and benign breast lesions and normal parenchyma in patients with breast lesions; and 3) assess the ability of the IVIM parameters and ADC to differentiate malignant lesions from benign lesions and FGT.

MATERIALS AND METHODS

Patient Selection

This retrospective study was compliant with the Health Insurance Portability and Accountability Act and approved by the local Institutional Review Board with a waiver of

informed consent. Consecutive patients were included in the study if they underwent bilateral breast MRI at 3.0 T at our institution between April 14 and August 21, 2011 for evaluation of biopsy-proven breast cancer and/or suspicious lesions, had DW MRI performed with at least nine b-values, were not receiving neoadjuvant chemotherapy or hormonal therapy at the time of imaging, and had their diagnosis confirmed by histopathology. Based on our selection criteria, 41 patients were identified and their MRI studies were reviewed by an experienced radiologist who had access to all patient information. In every patient, a single largest lesion in each breast was selected, resulting in 49 lesions (29 malignant and 20 benign). Lesions were excluded if their in-plane dimension was smaller than 8 mm ($n = 4$) or if their DW MR images contained artifacts, such as poor fat suppression or susceptibility artifacts from biopsy and surgical clips ($n = 5$). An experienced pathologist analyzed the biopsy specimens and identified the tumor histological type (25) as well as the tumor histological grade (26) and nuclear grade (27).

Additionally, we selected 20 consecutive subjects considered high risk who underwent screening breast MRI at 3.0 T, including DW MRI with 9 b-values, between April 22 and May 2, 2011. Four subjects were excluded (treatment, $n = 1$; artifacts, $n = 3$). Among the remaining 16 patients (mean age, 57 years; range, 41–75 years; premenopausal, $n = 6$ [38%]; postmenopausal, $n = 10$ [62%]), 10 had prior lumpectomies, eight had a family history of breast cancer, one had a history of mantle radiation therapy for Hodgkin's lymphoma, and one had hereditary breast and ovarian cancer syndrome. At the current MR examination, all were free from suspicious findings and received a score of 1 or 2 according to the Breast Imaging Reporting and Data System (BI-RADS) (28).

MR Image Acquisition

MRI was performed on a 3.0 T system (Discovery MR750; GE Healthcare, Waukesha, WI) using the body coil as a transmitter and a dedicated 16-channel phased-array receiver coil (Sentinelle Vanguard; Sentinelle Medical, Toronto, ON, Canada). Conventional T1- and T2-weighted images were acquired with and without fat suppression. Axial DW MRI was performed using DW single-shot dual spin echo sequence with echo-planar imaging readout at 9 b-values (b = 0, 30, 60, 90, 120, 400 [450 in seven cases], 600, 800, 1000 s/mm^2) with the parameters listed in Table 1. Dual shim volumes were placed over both breasts to optimize the B_0 homogeneity (29). Sagittal T1-weighted dynamic contrast-enhanced (DCE) MR images were acquired using volume image breast assessment (VIBRANT) gradient echo sequence before and at three points at 60-second intervals after an injection of 0.1 mmol/kg of gadopentetate dimeglumine (Magnevist; Bayer HealthCare Pharmaceuticals, Wayne, NJ). Axial T1-weighted CE images were acquired afterwards (Table 1). Parallel imaging using the array spatial sensitivity encoding technique (ASSET) was applied during acquisition of DW and CE MR images.

Image Analysis

Image analysis was performed in MatLab (MathWorks, Natick, MA). The ADC maps were calculated from the DW images at all b-values, assuming monoexponential signal shape:

$$S(b)=S_0\exp(-b\ ADC) \quad [1]$$

where b is the b-value and S_0 is the signal intensity at b = 0. The ADC maps were used primarily for locating the lesions and FGT. In the presence of the IVIM effect, the DW signal follows the biexponential dependence (3):

$$S(b)=S_0[f_p\exp(-bD_p)+(1-f_p)\exp(-bD_d)] \quad [2]$$

where f_p is the perfusion fraction, D_p is the pseudodiffusion coefficient, and D_d is the true diffusion coefficient. The parameters f_p, D_p, and D_d were estimated using the segmented approach proposed by Sigmund et al (24,30), which is preferable in our case, because the curve fitting of Eq. (2) to the signal intensity data acquired at relatively few b-values can result in large parameter uncertainties. First, the coefficient of true diffusion D_d was determined from the data within an interval of higher b-values, b_{mono}, where the IVIM component is negligible, using the least squares curve fit: $S_{mono}(b_{mono}) = S_{mono0}\exp(-b_{mono}D_d)$, where $S_{mono0} = S_0(1-f_p)$. The selection of the interval b_{mono} is described in the next subsection. Second, f_p was determined from the signal intensity at b = 0 s/mm^2 as $f_p = (S_0-S_{mono0})/S_0$. Third, D_p was obtained from the monoexponential fit to the difference between the data and the fit, $S - S_{mono}$. Finally, fitting curves were generated by substituting the estimated values of D_p, f_p, and D_d into Eq. (2). The goodness of fit was assessed using $R^2 = 1 - SSE/SS_{total}$, where SSE is the sum of squared errors between the data and the fitting curve and SS_{total} is the sum of squared differences between the data and the mean of all data values.

IVIM Parameters in High-Risk Normal Subjects—Based on the previous studies, normal FGT is not expected to show the IVIM effect (22,24). To ensure that our analysis does not create a spurious IVIM contribution, we analyzed the DW MR signal in the FGT of the high-risk normal subjects (FGT_N). In each subject a region of interest (ROI) was drawn on a single slice of the DW image at b = 120 s/mm^2 in the normal-appearing FGT, which was identified by high values of ADC and low enhancement on the CE images. Regions of fatty tissue with high intensity on T1-weighted nonfat-suppressed images were avoided. The mean ± standard deviation size of the ROIs was 83 ± 31 voxels (1.34 ± 0.48 cm^2). The IVIM parameters were estimated from the mean ROI signal intensity using the segmented method with 1) b_{mono} = [120,…,600] s/mm^2, and 2) b_{mono} = [400,…,800] s/mm^2. The DW signal curves were examined for the presence of the IVIM component, and the b-value interval b_{mono} that yielded the lowest f_p was chosen for subsequent analysis of the data in patients with lesions. The monoexponential ADC was determined using the least squares curve fit of Eq. (1) to the ROI signal at all b-values between b = 0 s/mm^2 and the maximum b-value of the b_{mono} interval.

IVIM Parameters in Breast Lesions—For each patient the radiologist identified the lesion on the axial T1-weighted CE images and marked the slice that contained the largest cross-section of the lesion. Two ROIs per patient, one over the lesion and the other in FGT, were drawn on DW images with b = 800 s/mm^2 on the slice that provided the closest match to the lesion location on CE MRI. The ROIs were drawn inside the tumor outline to avoid

the edge voxels affected by the motion and partial volume artifacts. In patients with bilateral lesions, FGT ROIs were drawn in each breast. For unilateral malignancy, FGT ROI was drawn in the contralateral breast and for patients with bilateral malignancy, FGT ROI was drawn in the ipsilateral breast but more than 2 cm away from the index lesion to avoid any influence of cancer extension. The size of the lesion ROIs was 89 ± 72 voxels (1.57 ± 1.30 cm^2), excluding four large tumors with the area greater than 300 voxels, and the FGT ROIs comprised 56 ± 40 voxels (1.00 ± 0.72 cm^2). The IVIM parameters and ADC were estimated for all lesion and FGT ROIs.

The sagittal DCE MR images were analyzed using commercial image processing software (Aegis; Hologic, Bedford, MA). The images were rendered in the axial plane and lesion ROIs were drawn at the levels matching the locations marked on the CE MR images. The initial upslope of enhancement was determined as the percent difference between the mean signal intensity values within the lesion ROI on the first postcontrast and the precontrast images (24).

Statistical Analysis

The parameters are presented as the mean ± standard deviation values. The parameters of bilateral lesions in the same patient were assumed to be uncorrelated. The Mann–Whitney *U*-test was used to compare the parameters of malignant and benign lesions, invasive ductal carcinoma (IDC) and non-IDC lesions, and lesions with masslike and nonmasslike enhancement. The Wilcoxon signed-rank test was applied to compare the parameters in lesions and FGT as well as the diffusivities (ADC and D_d) and the IVIM parameters estimated with different b_{mono} intervals in the same patient. The Spearman's correlation coefficient ρ was used to assess the correlation between the initial upslope of lesion enhancement on DCE MRI and the IVIM parameters.

The two-class classification of the ROIs based on their ADC and IVIM parameters (class 1: lesion of interest; class 2: other) was considered for the following classes: 1) malignant lesions versus benign lesions, 2) malignant lesions versus FGT in the same patients (denoted FGT_M), and 3) benign lesions versus FGT in the same patients (FGT_B). These classifications were tested for ADC, D_d, f_p individually and the combination of D_d and f_p, denoted (D_d, f_p). For (D_d, f_p), the classification was performed using the linear discriminant analysis (LDA) implemented as "classify" function in MatLab with prior probabilities equal to the relative frequencies of data in each class. The estimated posterior probability of belonging to class 1, ranging between 1 (definitely lesion of interest) and 0 (definitely other) was used as the discriminating parameter. The performance of each parameter was evaluated using the ROC analysis and the AUC, obtained from the "perfcurve" function in MatLab. The optimal sensitivity and specificity values were selected at the point on the ROC curve with the shortest distance to the (0,1) point, where both sensitivity and specificity are equal to unity. The standard error (SE) of the AUC and the statistical significance of the differences between the AUCs were determined using ROCKIT software (31). Statistical analysis, except the ROC comparison, was performed in MatLab's Statistics Toolbox. All statistical tests were two-tailed and statistical significance was established at $P = 0.05$.

RESULTS

The final dataset in this study comprised 40 lesions (26 malignant and 14 benign) in 35 women (mean age, 49 years; range, 28–70 years; premenopausal, $n = 24$ (69%); postmenopausal, $n = 11$ (31%)). The lesion characteristics are given in Table 2 for malignant lesions and in Table 3 for benign lesions. Among 24 patients with malignant lesions, 17 patients had a single lesion and two patients had bilateral malignancies: one patient had an invasive ductal carcinoma (IDC) and an invasive lobular carcinoma (ILC) and another patient had an IDC and a ductal carcinoma in situ (DCIS). Five patients had a malignant lesion in one breast and a benign lesion in the other breast (two of these benign lesions were excluded). Among 11 patients with benign lesions, 10 had unilateral lesions and one patient had bilateral lesions (one was excluded). In all patients the diagnosis was confirmed by biopsy.

IVIM Effect in High-Risk Normal Subjects

The high-risk normal subjects were older than the patients with lesions ($P = 0.019$) and a larger percentage of them were postmenopausal (62% versus 31% of patients with lesions); nevertheless, these subjects had ample amounts of FGT. The monoexponential fitting of the DW signal intensity in FGT_N at b = [0,…,600] s/mm^2 yielded $ADC_{600} = (2.18 \pm 0.19) \times 10^{-3}$ mm^2/s with $R^2 = 1.000$ in 14/16 subjects and $R^2 > 0.998$ in two remaining subjects (Fig. 1a). The IVIM analysis performed with b_{mono} = [120,…,600] s/mm^2 produced $f_p = 1.1 \pm 1.1\%$ and $D_d = (2.16 \pm 0.20) \times 10^{-3}$ mm^2/s. Because of the very low f_p, the values of D_p were highly variable ($(9.7 \pm 10.5) \times 10^{-3}$ mm^2/s). The parameters obtained in high-risk patients are summarized in Table 4.

The IVIM analysis with b_{mono} = [400,…,800] s/mm^2 yielded a slightly lower D_d ($(2.06 \pm 0.24) \times 10^{-3}$ mm^2/s, $P = 0.24$) and a significantly higher $f_p = 5.6 \pm 3.2\%$ ($P < 0.001$). In 11/16 subjects the DW signal at b>600 s/mm^2 deviated from the monoexponential shape and showed a slower decay (Fig. 1b), especially in the ROIs with lower diffusivity (Fig. 1c). Similar signal distortion has been previously observed in breast FGT at b>600 s/mm^2 by Baron et al (22). Based on these observations, the IVIM analysis in subjects with lesions was performed using b_{mono} = [120,…,600] s/mm^2.

IVIM Parameters in Patients With Breast Lesions

IVIM Parameters in Malignant Lesions—Examples of the T1-weighted CE images, DW images, ADC maps, and DW signals with the IVIM fits are shown in Fig. 2 for four malignant lesions of different histological types. The mean parameters of malignant lesions are given in Table 4. The mean f_p values in malignant lesions were significantly higher than in FGT_M ($P < 0.001$) and both ADC_{600} and D_d were significantly lower than in FGT_M ($P < 0.001$). Using the maximum value of f_p in FGT_M (~4.0%) as an empirical cutoff, $f_p > 4.0\%$ was detected in 21/26 (81%) of malignant lesions. The five lesions with $f_p \leq 4.0\%$ included two IDC lesions (nonmass), two ILC lesions and one DCIS lesion. In two patients with bilateral malignancies, only the IDC lesions showed an appreciable IVIM effect (f_p~6–7%), but not the contralateral ILC and DCIS lesions (f_p<1%). The IDC lesions tended to have higher f_p and lower D_d and ADC_{600} values than the non-IDC lesions (f_p, $P = 0.16$; D_d, $P =$

0.085; ADC_{600}, $P = 0.097$) (Table 4). The majority of malignant lesions showed masslike enhancement at CE MRI (17/26, 65%), and masses tended to have higher f_p ($P = 0.071$) and lower ADC_{600} and D_d ($P = 0.21$ for both parameters) than nonmasslike lesions (Table 4).

IVIM Parameters in Benign Lesions—Examples of images and IVIM analysis for four benign lesions are shown in Fig. 3. Only 3/14 benign lesions were high-risk (lobular carcinoma in situ (LCIS), $n = 2$; atypical ductal hyperplasia (ADH), $n = 1$). Among the benign lesions, 4/14 (29%) showed $f_p > 4\%$ (LCIS, $n = 2$; adenosis, $n = 1$; intraductal papilloma, $n = 1$) and 10/14 (71%) lesions had $f_p \leq 4\%$ (fibrocystic changes, $n = 3$; pseudoangiomatous ductal hyperplasia [PASH], ADH, columnar cell changes, fibrofatty tissue, intraductal papilloma, periductal inflammation, and benign parenchyma, $n = 1$ for each type). In both LCIS lesions, the values of f_p (8.1% and 11.1%) were comparable to their typical values in malignant lesions, but ADH had a lower f_p (3.2%). Benign lesions had a lower D_d than FGT_B ($P = 0.044$), but the differences in ADC_{600} ($P = 0.068$) and f_p ($P = 0.15$) were not statistically significant (Table 4). Benign lesions were significantly smaller than malignant lesions ($P = 0.003$) and, as a result, their DW signal was more strongly affected by the motion and partial volume artifacts.

IVIM Parameters Versus DCE MRI Parameters—There was a significant negative correlation between the initial upslope of enhancement and D_d when all lesions were combined ($\rho = -0.36$, $P = 0.03$), but did not reach significance for malignant lesions ($\rho = -0.30$, $P = 0.15$), or benign lesions ($\rho -0.17$, $P = 0.59$) taken separately. Similar correlations were found between the upslope and ADC for all lesions ($\rho = -0.38$, $P = 0.02$), malignant lesions ($\rho = -0.32$, $P = 0.12$), and benign lesions ($\rho = -0.13$, $P = 0.69$). The correlation between f_p and the initial upslope of enhancement was not significant for either malignant or benign lesions or both groups combined ($P > 0.43$).

Differentiation of Breast Lesions Based on ADC and the IVIM Parameters

The values of ADC_{600} and the IVIM within all ROIs are shown in Fig. 4 and the mean parameters for all tissues are summarized in Table 4. The parameters of FGT were not significantly different among breasts harboring malignant and benign lesions ($P > 0.26$ for all parameters), and the FGT ROIs of all patients with lesions were pooled together and denoted FGT_L. Both ADC_{600} and D_d in the FGT of the high-risk normal patients were significantly higher than in the FGT of the patients with lesions (ADC_{600}, $P = 0.032$; D_d, $P = 0.019$), owing to the larger amount of glandular tissue found in this set of normal subjects. Malignant lesions had significantly lower ADC_{600} ($P = 0.022$), lower D_d ($P = 0.011$), and higher f_p ($P = 0.0025$) than benign lesions, but D_p was highly variable and not significantly different between the two groups of lesions ($P = 0.36$). The diffusion coefficients ADC_{600} and D_d were strongly correlated ($\rho = 0.99$, $P < 0.001$ for all ROIs) and ADC_{600} was significantly higher than D_d in all tissue groups (malignant lesions, $P < 0.001$; benign lesions, $P = 0.028$; FGT_L, $P < 0.001$; FGT_N, $P = 0.005$). As expected, the difference between ADC_{600} and D_d was proportional to f_p ($\rho = 0.96$, $P < 0.001$, for all ROIs combined) (13,23).

The results of the ROC analysis for differentiation of malignant lesions from benign lesions, malignant lesions from FGT_M, and benign lesions from FGT_B are summarized in Table 5. Figure 5 illustrates the separation between the IVIM parameters for each pair of tissues in the scatterplot of f_p versus D_d (32) and the LDA-derived probability of belonging to the lesion of interest class for each ROI. For all three studied classifications, the combination (D_d, f_p) provided higher AUC than ADC_{600}, although the difference was statistically significant only for the discrimination of malignant lesions from FGT_M. For differentiation between malignant and benign lesions, at the optimal point on the ROC curve, D_d provided higher sensitivity compared to ADC_{600} by correctly identifying four more malignant lesions with relatively high f_p (f_p ~6–8%) that were classified as false negatives by ADC_{600}. A slight loss of specificity based on D_d resulted from one additional false-positive benign lesion (LCIS) with high f_p (f_p = 11.0%). The classification based on f_p provided both higher sensitivity and specificity than ADC_{600}. Lesions misclassified based on f_p at the optimal point of ROC included two false positives (both LCIS, f_p >8.0%) and seven false negatives, including three malignant lesions with $f_p \leq 2.2\%$ (IDC, ILC and DCIS) and four malignant lesions with $4.0\% \leq f_p \leq 4.8\%$ (all IDC). Finally, the combination of (D_d, f_p) was also superior to ADC_{600} in terms of both sensitivity and specificity. At the optimal probability cutoff, there were two false positives with high f_p (one LCIS lesion and one adenosis lesion) and four false negatives with low f_p and high D_d (two IDC, one ILC, and one DCIS).

For differentiation between malignant lesions and FGT_M, a significantly higher AUC for differentiation of cancer from FGT_M was obtained using D_d (P = 0.008) and (D_d, f_p) (P = 0.045) and both sensitivity and specificity at the optimal point were increased compared to the discrimination based on ADC_{600} (Table 5, Fig. 5c,d). Four malignant lesions could not be differentiated from FGT_M (the same lesions with low f_p and high D_d that could not be separated from the benign lesions), but only one FGT_M ROI was classified as a false positive based on (D_d, f_p). The advantage of using the IVIM parameters was less pronounced in differentiation between the benign lesions and FGT_B. This classification based on the IVIM parameters was limited by a large overlap between the diffusion coefficients of the benign lesions and FGT_B and by a large proportion of benign lesions with low f_p values (Fig. 5e,f).

DISCUSSION

We estimated the IVIM effect in malignant and benign breast lesions and normal breast parenchyma. Previous reports have stated that the IVIM effect in breast parenchyma is small, but did not specify the value of the perfusion fraction in FGT (24,33). We found that in 82% of ROIs in high-risk normal subjects and in 75% of ROIs in patients with lesions, the perfusion fraction in FGT did not exceed 2%. This finding is consistent with the low blood volume in breast tissue determined using imaging methods (34). The diffusion coefficients ADC_{600} and D_d obtained in this study were in agreement with the literature (15).

We observed that the IVIM parameters are affected by the choice of the b-value interval. It has been previously shown that this dependence results from the deviation of the DW signal from the monoexponential shape at high b-values (11,15,32). In FGT of the high-risk normal subjects, the DW signal was monoexponential up to b = 600 s/mm^2, but flattened at higher

b-values, especially in the ROIs with lower diffusivity (Fig. 1a,b). A similar distortion of the DW signal in FGT has been reported by Baron et al (22) and was shown to depend on the fat suppression method. When the segmented approach is used to estimate the IVIM parameters (24,30,35), including the high b-value data that are affected by this distortion, overestimation of the perfusion fraction may result. In normal subjects, when D_d was estimated from the interval b_{mono} = [400,…,800] s/mm^2, a 5-fold higher f_p was obtained than when b_{mono} = [120,…,600] s/mm^2 was used. Estimating the true diffusion coefficient D_d from the signal intensities at higher b-values may be desirable, because these data are less affected by the perfusion-related contribution; however, when the signal in this range is nonmonoexponential, the segmented approach should be applied with care in order to avoid the bias in the IVIM parameters.

We observed the IVIM effect with the perfusion fraction f_p greater than 4% in 81% of malignant lesions. The average perfusion fraction f_p in malignant lesions was lower than the values of f_p obtained by Sigmund et al in a similar set of malignant breast tumors (24). Besides the interpatient variability, the lower perfusion fraction obtained in our study can be explained by several factors. The shorter TE in our acquisitions (TE < 100 msec in 75% of cases) compared to the TE = 103 msec used by Sigmund et al (24) may have resulted in lower f_p values, as shown by Lemke et al (36). Furthermore, in this study, the lesion ROIs excluded the tumor edges. This was done to minimize the partial volume and motion artifacts and reduce the scatter in DW signal curves that might lead to errors in the IVIM parameters, but may have also yielded a lower perfusion fraction, because the tumor periphery is usually more vascularized than the tumor center. The difference between f_p in the IDC and non-IDC lesions (P = 0.16) in our data was less pronounced than in the study of Sigmund et al (P = 0.06) (24). We also observed a trend towards higher f_p in lesions with masslike enhancement compared to nonmasslike lesions (P = 0.071), which is consistent with the differences between these lesion types seen on DCE MRI and which may influence the accuracy of discrimination of the masslike lesions on DW MRI (37,38).

The diffusion coefficients of benign lesions were in agreement with the literature (15,17–19) and overlapped considerably with the diffusion coefficients of malignant lesions and FGT. Only three benign lesions in our dataset were high-risk lesions (two LCIS and one ADH lesion), and in both LCIS lesions the values of f_p were comparable to those found in malignant lesions. In the majority of benign lesions, f_p did not exceed 4%. This suggests that the IVIM parameters may help differentiate the benign lesions from malignant lesions based on their vascular properties, and further studies are warranted to test the usefulness of the IVIM parameters in distinguishing the high-risk benign lesions from other benign lesions.

We found no correlation between the lesions' f_p values and the initial upslope of contrast enhancement, whereas a moderate correlation between these parameters (Pearson's coefficient R = 0.42) was obtained by Sigmund et al in malignant lesions (24). We observed a negative correlation between D_d and the upslope of enhancement in all lesions compared to R = −0.27 found by Sigmund et al in cancer, which may reflect the coexistence of higher cellularity and higher vascularity in the more aggressive lesions.

The main advantage of using the IVIM parameters rather than ADC_{600} for lesion classification is the improved differentiation of malignant lesions. Using D_d increases the sensitivity of differentiation of malignant lesions from benign tissues. The IVIM component artificially increases the ADC values in proportion to f_p and often brings the ADCs of malignant lesions closer to the ADCs in benign tissues. Measuring D_d reduces this bias and helps to identify malignant lesions. Measurements of f_p increase the specificity of differentiation mainly by correctly identifying benign tissues with small IVIM component, as illustrated by the perfect specificity of differentiation of malignant lesions from FGT_M using f_p. The combination (D_d, f_p) takes advantage of the respective strengths of each parameter and improves both the sensitivity and specificity. In our dataset, the classification sensitivity was limited by the presence of malignant lesions with small f_p and relatively high D_d, which were classified as false negatives (two IDC, one ILC, and one DCIS. The specificity was limited by the presence of three benign lesions classified as false positives based on their high values of f_p, including two LCIS lesions and one adenosis lesion. Note that in this study the benign lesions were primarily represented by the low-risk lesions, and the discrimination of high-risk benign lesions based on their IVIM parameters needs to be further investigated.

Our study had the following limitations. First, our study was retrospective and the acquisition parameters and the b-values were not optimized, which may be a source of bias and variability in the IVIM parameter values, particularly f_p (36,39,40). Second, our dataset was small and included malignant and primarily low-risk benign lesions. Third, the IVIM analysis was performed by observers who had access to patient information. Finally, the analysis was performed on an ROI basis and the results may be dependent on the ROI selection.

In conclusion, the novel findings of this study demonstrated that 1) the IVIM effect is significantly larger in malignant breast lesions than in benign lesions and normal breast parenchyma, and 2) the IVIM parameters may improve the accuracy of breast cancer differentiation from benign tissues. The feasibility of the IVIM voxel analysis and the usefulness of IVIM parameters for lesion differentiation in different patient subpopulations need to be further investigated.

Acknowledgments

We thank Dr. Nathan Yanasak, Dr. Yonggang Lu, and Dr. Eric Sigmund for their valuable comments and suggestions. We also want to thank Dr. Sanjay Annarao for his technical assistance.

References

1. Padhani AR, Liu G, Koh DM, et al. Diffusion-weighted magnetic resonance imaging as a cancer biomarker: consensus and recommendations. Neoplasia. 2009; 11:102–125. [PubMed: 19186405]
2. Le Bihan D, Breton E, Lallemand D, Grenier P, Cabanis E, Laval-Jeantet M. MR imaging of intravoxel incoherent motions: application to diffusion and perfusion in neurologic disorders. Radiology. 1986; 161:401–407. [PubMed: 3763909]
3. Le Bihan D, Breton E, Lallemand D, Aubin ML, Vignaud J, Laval-Jeantet M. Separation of diffusion and perfusion in intravoxel incoherent motion MR imaging. Radiology. 1988; 168:497–505. [PubMed: 3393671]

4. Luciani A, Vignaud A, Cavet M, et al. Liver cirrhosis: intravoxel incoherent motion MR imaging—pilot study. Radiology. 2008; 249:891–899. [PubMed: 19011186]
5. Lemke A, Laun FB, Klauss M, et al. Differentiation of pancreas carcinoma from healthy pancreatic tissue using multiple b-values: comparison of apparent diffusion coefficient and intravoxel incoherent motion derived parameters. Invest Radiol. 2009; 44:769–775. [PubMed: 19838121]
6. Thoeny HC, Zumstein D, Simon-Zoula S, et al. Functional evaluation of transplanted kidneys with diffusion-weighted and BOLD MR imaging: initial experience. Radiology. 2006; 241:812–821. [PubMed: 17114628]
7. Morvan D. In vivo measurement of diffusion and pseudo-diffusion in skeletal muscle at rest and after exercise. Magn Reson Imaging. 1995; 13:193–199. [PubMed: 7739360]
8. Moore RJ, Issa B, Tokarczuk P, et al. In vivo intravoxel incoherent motion measurements in the human placenta using echo-planar imaging at 0.5 T. Magn Reson Med. 2000; 43:295–302. [PubMed: 10680695]
9. Yamada I, Aung W, Himeno Y, Nakagawa T, Shibuya H. Diffusion coefficients in abdominal organs and hepatic lesions: evaluation with intravoxel incoherent motion echo-planar MR imaging. Radiology. 1999; 210:617–623. [PubMed: 10207458]
10. Pang Y, Turkbey B, Bernardo M, et al. Intravoxel incoherent motion MR imaging for prostate cancer: an evaluation of perfusion fraction and diffusion coefficient derived from different b-value combinations. Magn Reson Med. 2013; 69:553–562. [PubMed: 22488794]
11. Lu Y, Jansen JF, Mazaheri Y, Stambuk HE, Koutcher JA, Shukla-Dave A. Extension of the intravoxel incoherent motion model to non-Gaussian diffusion in head and neck cancer. J Magn Reson Imaging. 2012; 36:1088–1096. [PubMed: 22826198]
12. Sumi M, Van Cauteren M, Sumi T, Obara M, Ichikawa Y, Nakamura T. Salivary gland tumors: use of intravoxel incoherent motion MR imaging for assessment of diffusion and perfusion for the differentiation of benign from malignant tumors. Radiology. 2012; 263:770–777. [PubMed: 22447854]
13. Woodhams R, Ramadan S, Stanwell P, et al. Diffusion-weighted imaging of the breast: principles and clinical applications. Radiographics. 2011; 31:1059–1084. [PubMed: 21768239]
14. Zhang JL, Sigmund EE, Chandarana H, et al. Variability of renal apparent diffusion coefficients: limitations of the monoexponential model for diffusion quantification. Radiology. 2010; 254:783–792. [PubMed: 20089719]
15. Bogner W, Gruber S, Pinker K, et al. Diffusion-weighted MR for differentiation of breast lesions at 3.0 T: how does selection of diffusion protocols affect diagnosis? Radiology. 2009; 253:341–351. [PubMed: 19703869]
16. Buadu LD, Murakami J, Murayama S, et al. Breast lesions: correlation of contrast medium enhancement patterns on MR images with histopathologic findings and tumor angiogenesis. Radiology. 1996; 200:639–649. [PubMed: 8756909]
17. Guo Y, Cai YQ, Cai ZL, et al. Differentiation of clinically benign and malignant breast lesions using diffusion-weighted imaging. J Magn Reson Imaging. 2002; 16:172–178. [PubMed: 12203765]
18. Woodhams R, Matsunaga K, Kan S, et al. ADC mapping of benign and malignant breast tumors. Magn Reson Med Sci. 2005; 4:35–42. [PubMed: 16127252]
19. Rubesova E, Grell AS, De Maertelaer V, Metens T, Chao SL, Lemort M. Quantitative diffusion imaging in breast cancer: a clinical prospective study. J Magn Reson Imaging. 2006; 24:319–324. [PubMed: 16786565]
20. Lo GG, Ai V, Chan JK, et al. Diffusion-weighted magnetic resonance imaging of breast lesions: first experiences at 3 T. J Comput Assist Tomogr. 2009; 33:63–69. [PubMed: 19188787]
21. Partridge SC, DeMartini WB, Kurland BF, Eby PR, White SW, Lehman CD. Quantitative diffusion-weighted imaging as an adjunct to conventional breast MRI for improved positive predictive value. AJR Am J Roentgenol. 2009; 193:1716–1722. [PubMed: 19933670]
22. Baron P, Dorrius MD, Kappert P, Oudkerk M, Sijens PE. Diffusion-weighted imaging of normal fibroglandular breast tissue: influence of microperfusion and fat suppression technique on the apparent diffusion coefficient. NMR Biomed. 2010; 23:399–405. [PubMed: 20131313]

23. Sinha S, Lucas-Quesada FA, Sinha U, DeBruhl N, Bassett LW. In vivo diffusion-weighted MRI of the breast: potential for lesion characterization. J Magn Reson Imaging. 2002; 15:693–704. [PubMed: 12112520]
24. Sigmund EE, Cho GY, Kim S, et al. Intravoxel incoherent motion imaging of tumor microenvironment in locally advanced breast cancer. Magn Reson Med. 2011; 65:1437–1447. [PubMed: 21287591]
25. Lakhani, SR.; Ellis, IO.; Schnitt, SJ.; Tan, PH.; van de Vijver, MJ. WHO Classification of Tumors of the Breast (IARC WHO Classification of Tumors). Geneva: World Health Organization; 2012.
26. Elston CW, Ellis IO. Pathological prognostic factors in breast cancer. I. The value of histological grade in breast cancer: experience from a large study with long-term follow-up. Histopathology. 1991; 19:403–410. [PubMed: 1757079]
27. Cutler SJ, Black MM, Mork T, Harvei S, Freeman C. Further observations on prognostic factors in cancer of the female breast. Cancer. 1969; 24:653–667. [PubMed: 4309690]
28. American College of Radiology. Breast imaging reporting and data system (BI-RADS). Reston, VA: American College of Radiology; 2003.
29. Hancu I, Govenkar A, Lenkinski RE, Lee SK. On shimming approaches in 3T breast MRI. Magn Reson Med. 2012; 69:862–867. [PubMed: 22556115]
30. Sigmund EE, Vivier PH, Sui D, et al. Intravoxel incoherent motion and diffusion-tensor imaging in renal tissue under hydration and furosemide flow challenges. Radiology. 2012; 263:758–769. [PubMed: 22523327]
31. Metz CE.ROC software. Department of Radiology, University of Chicago Medical Center. 2006. Available at: http://metz-roc.uchicago.edu/MetzROC/Accessed May 30, 2012
32. Pang Y, Turkbey B, Bernardo M, et al. Intravoxel incoherent motion MR imaging for prostate cancer: an evaluation of perfusion fraction and diffusion coefficient derived from different b-value combinations. Magn Reson Med. 2013; 69:553–562. [PubMed: 22488794]
33. Morris EA, Liberman L, Ballon DJ, et al. MRI of occult breast carcinoma in a high-risk population. AJR Am J Roentgenol. 2003; 181:619–626. [PubMed: 12933450]
34. Delille JP, Slanetz PJ, Yeh ED, Kopans DB, Garrido L. Breast cancer: regional blood flow and blood volume measured with magnetic susceptibility-based MR imaging—initial results. Radiology. 2002; 223:558–565. [PubMed: 11997568]
35. Kim S, Decarlo L, Cho GY, et al. Interstitial fluid pressure correlates with intravoxel incoherent motion imaging metrics in a mouse mammary carcinoma model. NMR Biomed. 2012; 25:787–794. [PubMed: 22072561]
36. Lemke A, Laun FB, Simon D, Stieltjes B, Schad LR. An in vivo verification of the intravoxel incoherent motion effect in diffusion-weighted imaging of the abdomen. Magn Reson Med. 2010; 64:1580–1585. [PubMed: 20665824]
37. Jansen SA, Fan X, Karczmar GS, et al. DCEMRI of breast lesions: is kinetic analysis equally effective for both mass and nonmasslike enhancement? Med Phys. 2008; 35:3102–3109. [PubMed: 18697535]
38. Partridge SC, Mullins CD, Kurland BF, et al. Apparent diffusion coefficient values for discriminating benign and malignant breast MRI lesions: effects of lesion type and size. AJR Am J Roentgenol. 2010; 194:1664–1673. [PubMed: 20489111]
39. Lemke A, Stieltjes B, Schad LR, Laun FB. Toward an optimal distribution of b values for intravoxel incoherent motion imaging. Magn Reson Imaging. 2011; 29:766–776. [PubMed: 21549538]
40. Zhang JL, Sigmund EE, Rusinek H, et al. Optimization of b-value sampling for diffusion-weighted imaging of the kidney. Magn Reson Med. 2012; 67:89–97. [PubMed: 21702062]

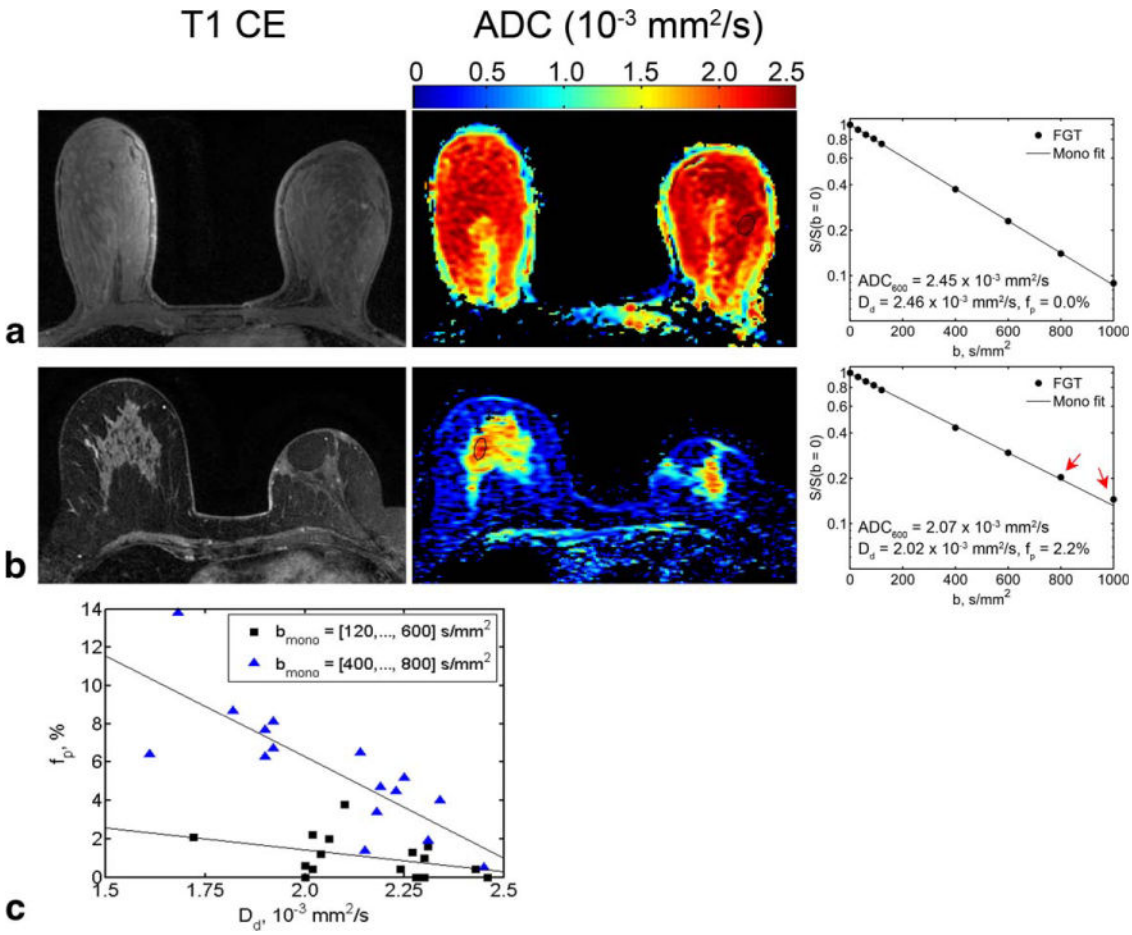

Figure 1.

The IVIM effect in high-risk normal subjects: T1-weighted CE images, ADC maps, DW signal intensity curves, and monoexponential fits. **a**: 50-year-old patient with extremely dense breasts, postleft lumpectomy. The DW signal at b ≤ 600 s/mm^2 yields ADC_{600} = 2.45 × 10^{-3} mm^2/s, R^2 = 1.000 and shows no IVIM effect (b_{mono} = [120,…,600] s/mm^2, f_p = 0%, D_d = 2.46 × 10^{-3} mm^2/s). The signal remains virtually monoexponential up to b = 1000 s/mm^2 (b_{mono} = [400,…800] s/mm^2 f_p = 1.0%, D_d = 2.45 × 10^{-3} mm^2/s). **b**: A 65-year-old patient with breasts composed of scattered fibroglandular elements, post-left lumpectomy. The DW signal is monoexponential up to b = 600 s/mm^2 (ADC_{600} = 2.07 × 10^{-3} mm^2/s, R^2 = 1.000; f_p = 2.2%, D_d = 2.02 × 10^{-3} mm^2/s), but flattens at b ≥ 800 s/mm^2 (red arrows). The IVIM analysis with b_{mono} = [400,…800] s/mm^2 yields f_p = 7.7% and D_d = 1.90 ×10^{-3} mm^2/s. c: Scatterplot of f_p versus D_d in all high-risk patients (*n* = 16). The data are derived from the IVIM analyses performed with 1) b_{mono} = [120,…,600] s/mm^2 (black squares), and 2) b_{mono} = [400,…800] s/mm^2 (blue triangles). Although none of the FGT signal curves shows an appreciable IVIM contribution, using larger b-values to determine D_d leads to an overestimation of f_p. This overestimation is greater for ROIs with lower diffusivities, as indicated by the slopes of the linear regression lines (solid lines) in **(c)**. [Color figure can be viewed in the online issue, which is available at wileyonlinelibrary.com.]

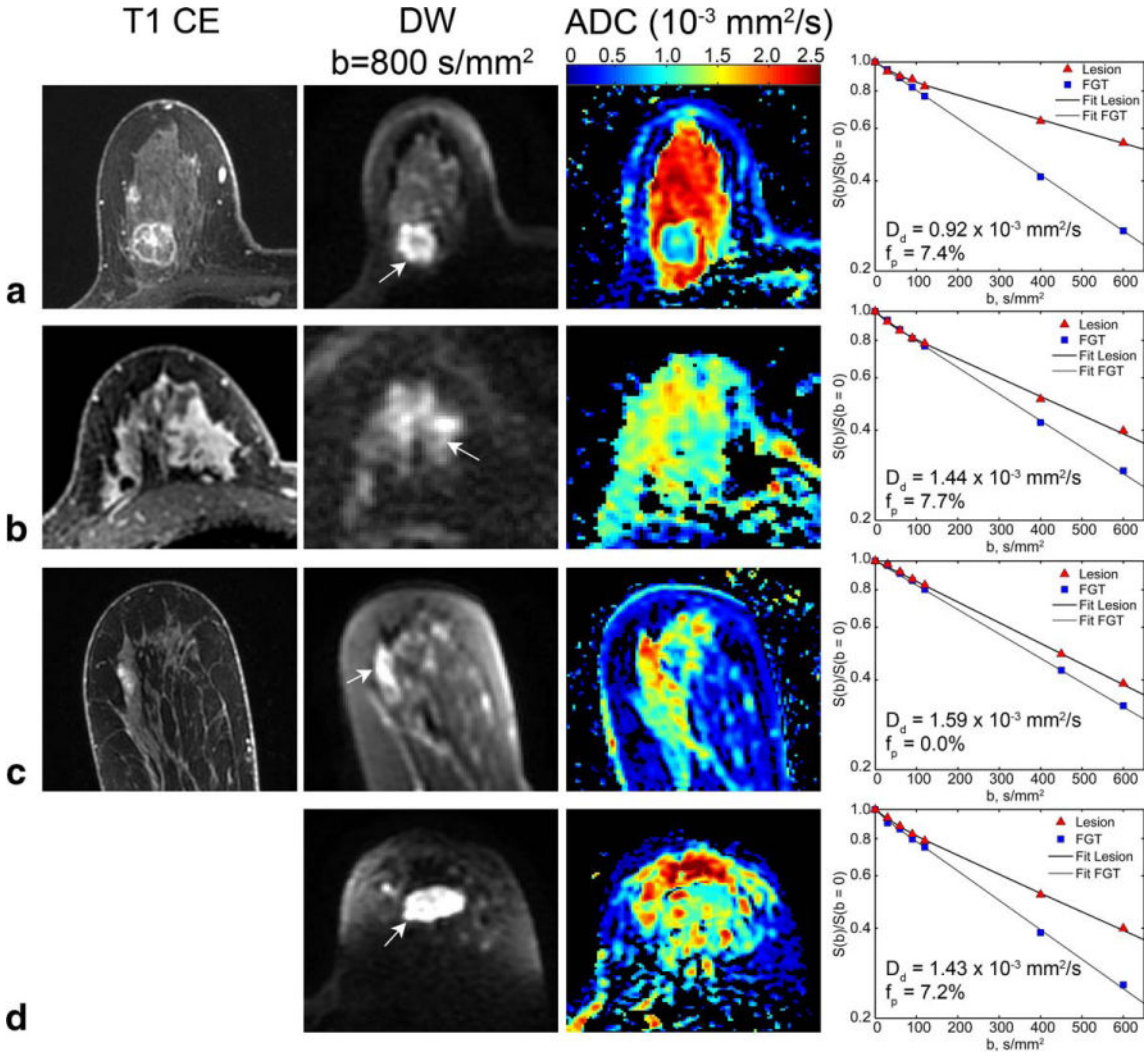

Figure 2.

The IVIM effect in malignant lesions: T1-weighted CE images, DW images at b = 800 s/mm^2, ADC maps and DW ROI signals for lesions and FGT and IVIM fits. **a**: A 67-year-old patient with IDC (25 mm). **b**: A 51-year-old patient with ILC (26 mm). **c**: A 70-year-old patient with DCIS (14 mm). **d**: A 48-year-old patient with invasive metaplastic squamous cell carcinoma (52 mm). White arrows indicate the lesions on DW images. Images were scaled arbitrarily. In **(d)** the T1-weighted CE MR images were not available because the patient could not tolerate the gadolinium contrast. This case represents a potential application of IVIM measurements as an auxiliary technique when CE MRI cannot be performed.

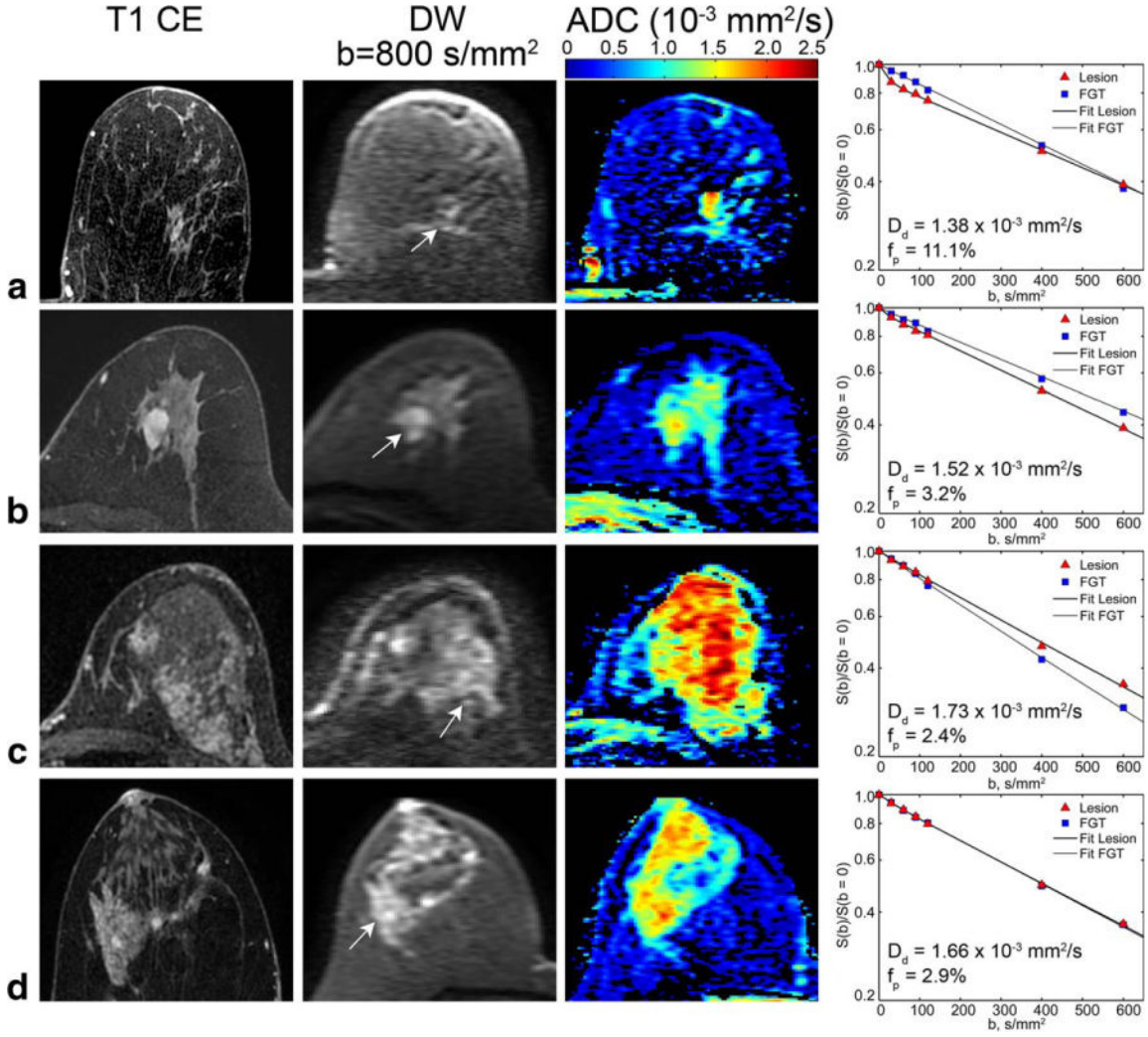

Figure 3.

The IVIM effect in benign lesions. T1 CE images, DW images, ADC maps, and DW signal with the IVIM fits and parameters for four tumors. **a**: A 41-year-old patient with lobular carcinoma in situ (diameter, 10 mm). **b**: A 42-year-old patient with atypical ductal hyperplasia (19 mm). **c**: A 43-year-old patient with pseudoangiomatous stromal hyperplasia (23 mm). **d**: A 49-year-old patient with columnar cell changes (48 mm). White arrows indicate the lesions on DW images. Images were scaled arbitrarily.

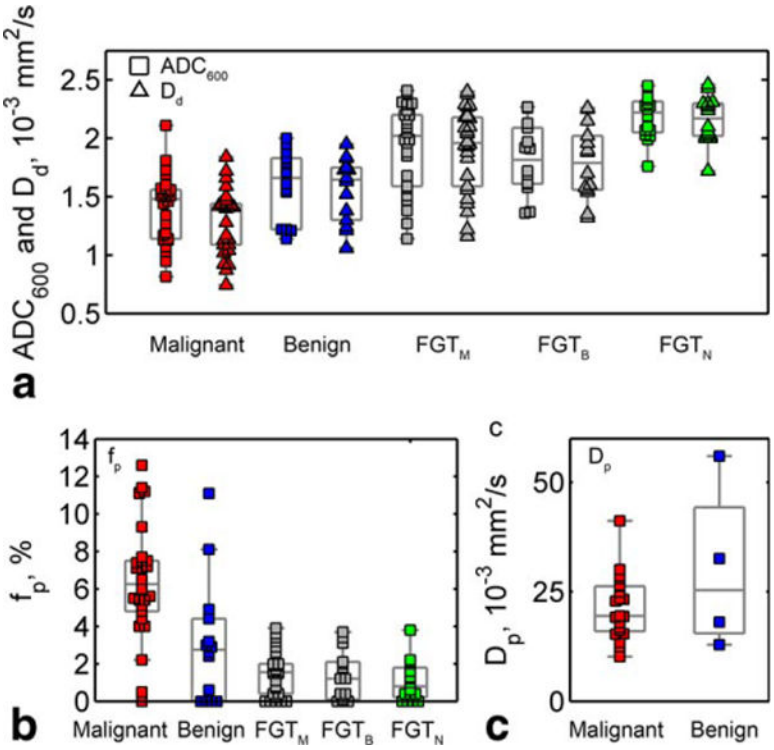

Figure 4.

Boxplots of (**a**) ADC_{600} and D_d, (**b**) f_p, and (**c**) D_p. In (**a,b**), symbols represent individual values for all ROIs in malignant lesions, benign lesions and FGT in patients with malignant lesions (FGT_M) and benign lesions (FGT_B) and high-risk normal patients (FGT_N). In (**c**), D_p is shown only for malignant and benign lesions with $f_p > 4.0\%$. The horizontal lines in boxplots represent the median value and the lower and upper quartiles, and the whiskers span ± 1.5 × interquartile range. [Color figure can be viewed in the online issue, which is available at wileyonlinelibrary.com.]

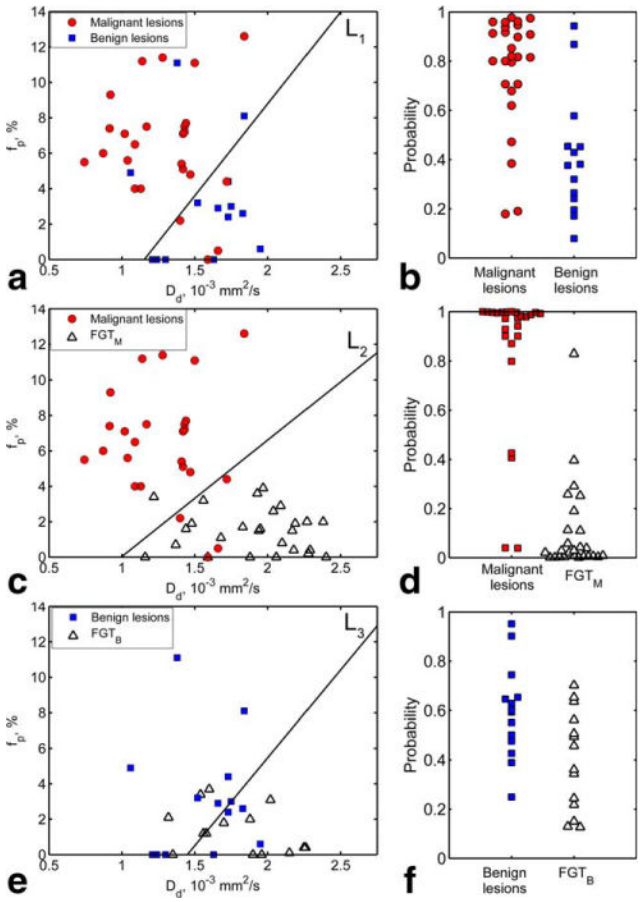

Figure 5.

Scatterplots of f_p versus D_d (left column) and the LDA-derived posterior probability (right column) of belonging to the lesion-of-interest class based on the combination of (D_d, f_p) for differentiation between: (**a,b**) malignant lesions and benign lesions, (**c,d**) malignant lesions and FGT_M, and (**e,f**) benign lesions and FGT_B. The solid lines in f_p versus D_d plots indicate the LDA decision boundaries: (**a**) $L_1 = -3.84 + 3.33 \times D_d/(10^{-3}\ mm^2/s) - 0.32 \times f_p/(1\%) = 0$; (**c**) $L_2 = -5.38 + 5.40 \times D_d/(10^{-3}\ mm^2/s) - 0.82 \times f_p/(1\%) = 0$, and (**e**) $L_3 = -3.63 + 2.51 \times D_d/(10^{-3}\ mm^2/s) - 0.25 \times f_p/(1\%) = 0$. [Color figure can be viewed in the online issue, which is available at wileyonlinelibrary.com.]

Table 1

MRI Acquisition Parameters

Parameter	DW MRI	DCE MRI	CE MRI
Sequence	2D DW single-shot dual spin echo EPI	3D T1-weighted gradient echo VIBRANT	3D T1-weighted gradient echo VIBRANT
Imaging plane	Axial	Sagittal	Axial
TR, ms	6000	9.89–11.83	4.30–5.11
TE, ms	56.4–120.7	2.1	2.1–2.39
Flip angle, degrees	90	10 or 15	10 or 15
Number of excitations	3	1	1
Acquisition matrix	98×98 (n = 15) or (n = 20) 128×128 (n = 20)	320×180 to 448×224	320×320 to 420×420
Reconstructed matrix	256×256	512×512	512×512
Field of view*, cm	28–38	20–25	28–38
Slice thickness, mm	5	3	0.8
Slice gap, mm	0–1	0	0
Number of slices	17–23	80–112	204–306
Fat suppression	Enhanced	On	On
Parallel imaging	ASSET	–	ASSET
b-values, s/mm^2	0, 30, 60, 90, 120, 400 (450 in 7 cases), 600, 800, 1000	–	–
Time per frame, s	–	60	–
Number of phases	–	4 (1 pre- and 3 post-contrast)	–
Acquisition time, min	5–6	8	1.5–2.5

EPI, echo-planar imaging; VIBRANT, Volume Image Breast Assessment; ASSET, array spatial sensitivity encoding technique; TR, repetition time; TE, echo time.

* Field of view was a square with the side length specified in the table.

Table 2

Characteristics of Malignant Lesions

Characteristic	Value
Total number	26
Maximum size at MR, mm, mean (range)	38 (9–80)
Histopathological type	
Invasive ductal carcinoma (IDC)	21 (81)
Other histology (non-IDC)	5 (19)
Invasive lobular carcinoma	3
Ductal carcinoma in situ	1
Invasive metaplastic squamous cell carcinoma	1
Lymph node metastases*	
Positive	12 (46)
Negative	12 (46)
Histological grade* (IDC lesions)	
I	4 (19)
II	6 (29)
III	10 (48)
Nuclear grade* (IDC lesions)	
I	1 (5)
II	10 (48)
III	9 (43)
Lesion enhancement type*	
Mass	17 (65)
Nonmass	8 (31)
Enhancement kinetic type*	
Washout	13 (50)
Plateau	11 (42)
Progressive	1 (4)

IDC, invasive ductal carcinoma. Data are numbers of patients (percentage), unless specified otherwise.

*Data unavailable: lymph node status (n = 2); histological grade (n = 1); nuclear grade (n = 1); contrast-enhanced examination (n = 1, invasive metaplastic squamous cell carcinoma).

Table 3

Characteristics of Benign Lesions

Characteristic	Value
Total number	14
Maximum size, mm, mean (range)	20 (8–48)
Histopathological type	
Lobular carcinoma in situ	2 (14)
Atypical ductal hyperplasia	1 (7)
Intraductal papilloma	2 (14)
Pseudoangiomatous stromal hyperplasia	1 (7)
Columnar cell changes	1 (7)
Fibrocystic changes with ductal hyperplasia	3 (21)
Fibrofatty benign	1 (7)
Periductal inflammation	1 (7)
Benign with adenosis	1 (7)
Benign	1 (7)
Lesion enhancement type	
Mass	13 (93)
Nonmass	1 (7)
Enhancement type	
Washout	1 (7)
Plateau	11 (79)
Progressive	2 (14)

Data are numbers of patients (percentage), unless specified otherwise.

Table 4

Monoexponential ADC_{600} and the IVIM Parameters True Diffusion Coefficient D_d, Perfusion Fraction f_p, and Pseudodiffusion Coefficient D_p in Malignant and Benign Breast Lesions and FGT

Region of interest	ADC_{600}(10^{-3} mm^2/s)	D_d(10^{-3} mm^2/s)	f_p (%)	D_p(10^{-3} mm^2/s)
Malignant lesions (*n* = 26)	1.40 ± 0.30*,†	1.29 ± 0.28*,†	6.4 ± 3.1*,†	21.7 ± 11.0
IDC (*n* = 21)	1.37 ± 0.31	1.25 ± 0.29	7.0 ± 2.7	22.4 ± 8.6
Non-IDC (*n* = 5)	1.52 ± 0.20	1.45 ± 0.20	3.9 ± 3.6	18.7 ± 19.3
Mass (*n* = 17)	1.35 ± 0.33	1.24 ± 0.30	7.3 ± 2.6	24.1 ± 9.1
Nonmass (*n* = 8)	1.48 ± 0.22	1.39 ± 0.21	4.8 ± 3.6	17.0 ± 13.2
Benign lesions (*n* = 14)	1.60 ± 0.30	1.56 ± 0.28‡	3.1 ± 3.3	27.6 ± 34.0
FGT_M (*n* = 26)	1.93 ± 0.36	1.90 ± 0.36	1.5 ± 1.2	–
FGT_B (*n* = 14)	1.82 ± 0.30	1.79 ± 0.31	1.4 ± 1.3	–
FGT_L (*n* = 40)	1.89 ± 0.34§	1.86 ± 0.34§	1.5 ± 1.2	–
FGT_N (*n* = 16)	2.18 ± 0.19	2.16 ± 0.20	1.1 ± 1.1	–

ADC_{600}, apparent diffusion coefficient calculated from data at b = [0,…, 600] s/mm^2. Data are mean ± standard deviation values within each group of ROIs. FGT data are reported in patients with malignant lesions (FGT_M) and benign lesions (FGT_B), all patients with lesions (FGT_L), and high-risk normal patients (FGT_N). D_p values in FGT are not reported because of the low f_p values in normal parenchyma.

*Malignant lesions versus FGT_M: ADC_{600}, D_d, f_p, P < 0.001.

†Malignant lesions versus benign lesions: ADC_{600}, *P* = 0.022; D_d, *P* = 0.011; f_p, *P* = 0.0025.

‡Benign lesions versus FGT_B: D_d, *P* = 0.044.

§FGT_L versus FGT_N: ADC_{600}, *P* = 0.032; D_d, *P* = 0.019.

Table 5

Area Under Curve (AUC) and Standard Error (SE) of AUC for the ROC Curves for Differentiation of Breast Lesions Based on the Values of ADC_{600}, D_d, f_p and the Combination (D_d, f_p), Optimal Sensitivity and Specificity for Each Parameter and the Corresponding Parameter Thresholds

Parameter	AUC (SE)	Sensitivity	Specificity	Threshold
Malignant lesions versus benign lesions				
ADC_{600} (mm^2/s)	0.72 (0.08)	0.65	0.71	1.54×10^{-3}
D_d(mm^2/s)	0.75 (0.08)	0.85	0.64	1.52×10^{-3}
f_p (%)	0.79 (0.07)	0.73	0.86	4.9
(D_d, f_p) (probability, unitless)	0.84 (0.06)	0.85	0.86	0.58
Malignant lesions versus FGT_M				
ADC_{600} (mm^2/s)	0.86 (0.05)	0.77	0.81	1.57×10^{-3}
D_d (mm^2/s)	0.90 (0.04)*	0.81	0.85	1.48×10^{-3}
f_p (%)	0.93 (0.04)	0.88	1.00	3.9
(D_d, f_p) (probability, unitless)	0.97 (0.03)†	0.92	0.96	0.40
Benign lesions versus FGT_B				
ADC_{600} (mm^2/s)	0.69 (0.10)	0.86	0.50	1.91×10^{-3}
D_d (mm^2/s)	0.69 (0.10)	0.93	0.50	1.88×10^{-3}
f_p (%)	0.63 (0.11)	0.64	0.79	2.1
(D_d, f_p) (probability, unitless)	0.74 (0.10)	0.71	0.64	0.49

FGT_M and FGT_B are FGT ROIs in patients with malignant and benign lesions, respectively. The probability of belonging to the lesion of interest class based on (D_d, f_p) ranges between $P = 1$ (definitely tissue of interest) and $P = 0$ (definitely other).

*AUC(D_d) versus AUC(ADC_{600}): $P = 0.008$.

†AUC(D_d, f_p) versus AUC(ADC_{600}): $P = 0.045$.